Investigation of the unsteady pressure pulsations in the prototype Francis turbines - part 1: steady state operating conditions

Chirag Trivedi[1]

Postdoctoral Fellow, Waterpower Laboratory, Norwegian University of Science and Technology (NTNU), NO-7491 Trondheim, Norway. E-mail: chirag.trivedi@ntnu.no

Peter Joachim Gogstad

Ph. D. Candidate, Waterpower Laboratory, Norwegian University of Science and Technology (NTNU), NO-7491 Trondheim, Norway. E-mail: peter.j.gogstad@ntnu.no

Ole Gunnar Dahlhaug

Professor, Waterpower Laboratory, Norwegian University of Science and Technology (NTNU), NO-7491 Trondheim, Norway. E-mail: ole.g.dahlhaug@ntnu.no

ABSTRACT

Hydropower is one of the most reliable renewable sources of electricity generation. With high efficiency and good regulating capacity, hydropower has the ability to meet rapid changes in power demand. Large investments in intermittent renewable energy resources have increased the demand for balancing power. This demand has pushed hydraulic turbines to generate electricity over the operating range from part load to full load. High-amplitude pressure pulsations are developed at off-design conditions, which cause moderate damage to the turbine components. The pressure pulsations may be either synchronous- (axial)-type, asynchronous- (rotating)-type or both. In this study, pressure measurements on low specific-speed prototype Francis turbines were performed; one of them was vertical axis and another was horizontal axis type. Four pressure sensors were mounted on the surface of the draft tube cone. Pressure measurements were performed at five operating points. The investigations showed that, in the vertical axis turbine, amplitudes of asynchronous pressure pulsations were 20 times larger than those of the synchronous component; whereas, in the horizontal axis turbine, amplitudes of asynchronous pressure pulsations were two times smaller than those of the synchronous component.

Keywords: hydro turbine; pressure measurement; signal processing; spectral analysis; unsteady flow;

1. Introduction

Global electricity demand is met by both renewable and non-renewable energy sources. A hydropower source is one of the most stable sources of renewable energy used to generate electricity. Hydropower sources

[1] Author for correspondence. Postal address: Department of Energy and Process Engineering, Norwegian University of Science and Technology, NO-7491 Trondheim, Norway. Tel: +47 735 93849. E-mail: chirag.trivedi@ntnu.no

contribute more than 20% of generated energy globally [1]. The hydraulic turbine is an important component in a hydropower plant that converts available waterpower into mechanical power (torque). The mechanical power is used by a coupled generator to produce electricity. Hydraulic turbines are designed for given head and discharge conditions where the maximum efficiency of the turbine is obtained, known as the best efficiency point (BEP). The current trend of the electricity market does not allow hydraulic turbines to operate at the BEP constantly. The turbines are operated over the complete range of power generation, starting from part load to the full load [2].

Power generation at off-design conditions affect the dynamic stability of hydraulic turbines [3, 4]. High-amplitude pressure pulsations developed in a draft tube cause fatigue damage to the turbine [5, 6]. The pressure pulsations developed in a draft tube are related to the vortex breakdown. The pressure pulsations are composed of two different phenomena occurring simultaneously at the same frequency [7]. These pressure pulsations may be explained reasonably when a clear distinction between synchronous (axial) and asynchronous (radial) type pressure pulsations is made [7-10].

- The synchronous component may have equal phase and amplitude in the runner and the draft tube. The pressure may be considered as a plane wave propagating to hydraulic system through the draft tube.
- The asynchronous component is a pressure pattern developing at the runner downstream and rotating about the circumference of the draft tube. The rotation period is dependent upon the circumference and the runner angular speed.
- The synchronous component may not be present at high load conditions.

Both synchronous and asynchronous types of pressure pulsations cause different impacts on turbine operation. Therefore, it is important to analyze and distinguish the pressure pulsations. The majority of studies have investigated the draft tube flow condition of a model turbine [11-13]; however, no study has been reported on the investigation of synchronous- and asynchronous-type pressure pulsations in prototypes. Measurements on the model turbines are not completely representative of the prototype and its dynamic behavior [11, 14-17]. An isolated test facility available in the laboratory has different dynamic characteristics [5, 18] and has limited scope for scaling the data.

This paper discusses investigations conducted on prototype Francis turbines at five operating points. Four pressure sensors were mounted in the draft tube cone to acquire the unsteady pressure values. Low frequency pressure pulsations and decomposition into the synchronous and asynchronous components are of special interest in this paper. These pressure pulsations typically occur between 0.2 and 0.3 times the runner angular speed [18]. Moreover, repeated measurements at the same operating point were performed to study the randomness and repeatability of the results. The statistical behavior, spectral content, correlation among the pressure values, random noise and cross spectrum of the acquired time-series pressure values were studied. Moreover, variations in the pressure amplitudes with respect to the runner position were studied.

2. Materials and methods

Pressure measurements were conducted on two low head Francis turbines located at Leirfossen in Trondheim, Norway. The Francis turbine (turbine-1) located at Nedre Leirfossen was a vertical axis type with 2.5 MW of nominal power. The second turbine (turbine-2), located at Øvre Leirfossen, was a 3.5 MW horizontal axis Francis turbine. The locations of the pressure sensors for turbine-2 are shown in **Fig. 1**. The pressure sensors for turbine-2 were mounted at the same location as those for turbine-1. **Table 1** presents operating parameters of both turbines observed at the BEP. The speed factor (n_{ED}), discharge factor (Q_{ED}) and specific speed (N_{QE}) are estimated using Equations (1), (2) and (3), respectively [18]:

$$n_{ED} = \frac{n \cdot D}{E^{0.5}} \quad (-) \tag{1}$$

$$Q_{ED} = \frac{Q}{D^2 \cdot E^{0.5}} \quad (-) \tag{2}$$

$$N_{QE} = \frac{n \cdot Q^{0.5}}{E^{0.75}} \quad (-) \tag{3}$$

where n is the runner angular speed in revolutions per second (rps), D is the runner outlet diameter in m, Q is the discharge in $m^3\ s^{-1}$ and E is the specific hydraulic energy in $J\ kg^{-1}$. The specific speed of both of the turbines is 0.27. The runner outlet diameters for turbine-1 and turbine-2 are 1.389 and 1.334 m, respectively. Both turbines include 8 stay vanes, 16 guide vanes and 13 blades.

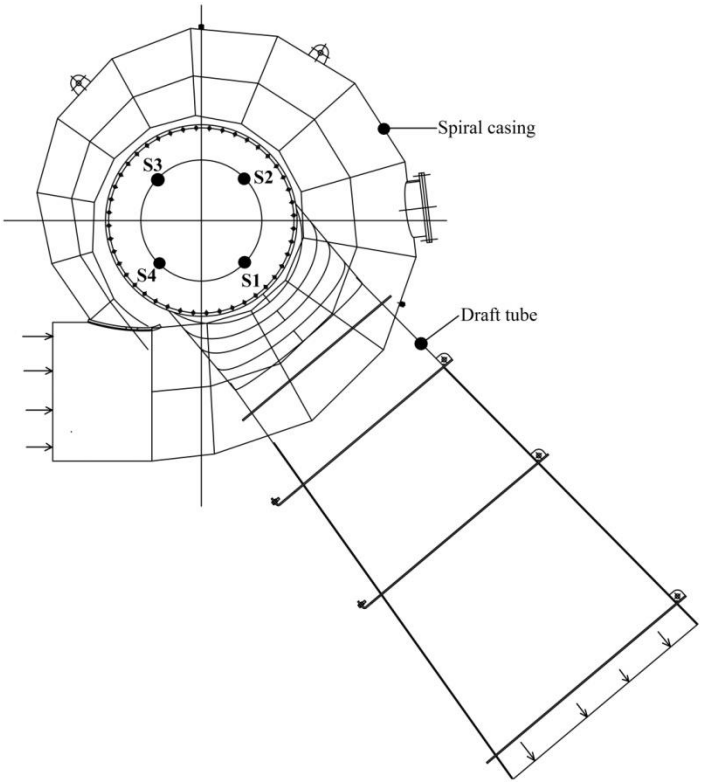

Fig. 1 Two-dimensional view of a prototype Francis turbine (horizontal axis). S1, S2, S3 and S4 are the locations of the pressure sensors in the draft tube cone.

Table 1 Operating parameters of the investigated Francis turbines

Parameter (symbol)	**Turbine-1**	**Turbine-2**	**Unit**
Head (H)	25.7	32.6	m
Discharge (Q)	10	10.5	$m^3\ s^{-1}$
Power (P)	2.5	3.5	MW
Efficiency (η)	94.7	91.7	%
Angular speed (n)	5.55	6.25	rps
Runner outlet diameter (D)	1.389	1.334	m
Speed factor (n_{ED})	0.49	0.47	-
Discharge factor (Q_{ED})	0.33	0.33	-
Specific speed (N_{QE})	0.27	0.27	-
Runner axis	Vertical	Horizontal	-

The pressure measurements were performed alongside an efficiency measurement of the turbines. Five operating points were investigated: 50%, 70%, 90%, 100% (BEP) and 110% of BEP load. The discharge was measured using pitot static tubes at four radial locations of the penstock. The headrace and tailrace levels were measured with respect to the reference height of the corresponding power plant. The turbine efficiency at the five operating points was calculated using the procedure available in the IEC standards [18, 19]. The results of efficiency measurements are not discussed in this paper due to confidentiality and an agreement with the power plant owner.

For the pressure measurements in the draft tube, four PTX 610 pressure transmitters (sensors) were mounted in the draft tube cone within the range of 0 – 250 kPa absolute. IEC 60193 recommends pressure measurements at a minimum of four locations [18]. The four pressure sensors were mounted at evenly spaced locations around the draft tube cone in one plane located at $0.27 \cdot D$ downstream of the runner outlet.

The pressure data were acquired through a National Instrument data acquisition system and a developed LabVIEW program. The data were sampled at the sampling rates of 100 Hz, 500 Hz, 1 kHz, 1.5 kHz and 2.5 kHz over 500 seconds for all the measurement series. This has allowed to verify the variation of frequencies and amplitudes of pressure fluctuations, if any, for different sampling rate. The frequency resolution is less than 0.05% of the runner angular speed.

3. Results and discussion

3.1 Pressure pulsations: Francis turbine-1

The average pressure values from sensor locations S1, S2, S3 and S4 are shown in **Fig. 2**. The highest average pressure is observed to be 94.5 kPa at 70% load, which is 0.3 kPa higher than at the minimum load (50% load). For loads higher than 70% load, the mean pressure decreases with increasing load. The average pressure at 70% load may be a result of the high-amplitude pressure pulsations. To investigate the variation in fluctuating pressure values, the standard deviation ($\tilde{p}_{\mathrm{eff}}$) of the acquired pressure values was computed. **Fig. 3** shows the standard deviation for each sensor at every load. The standard deviations for the 90%, 100% and 110% load operating conditions are less than 0.85 kPa (0.3% of head), indicating that the draft tube flow is relatively stable. The minimum standard deviation (< 0.7 kPa) is observed for 100% load, and the maximum standard deviation, i.e., 5.4 kPa (2.1% of head) is observed for the 70% load operating condition. Interestingly, the standard deviation at 50% load operating condition is only 4.2 kPa, which is 1.2 kPa lower than the standard deviation observed for the 70% load operating condition. The maximum value of standard deviation at the 70% load condition corresponds to the high-amplitude pressure pulsations in the draft tube.

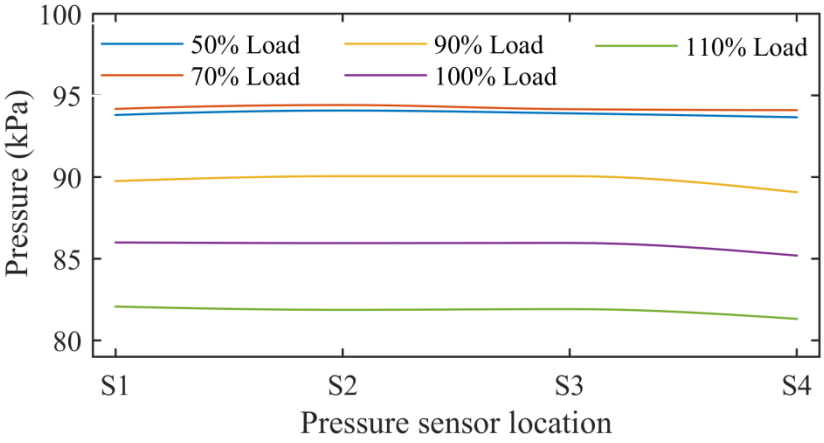

Fig. 2 Average pressure loading at locations S1, S2, S3 and S4 at the 50%, 70%, 90%, 100% and 110% load operating conditions.

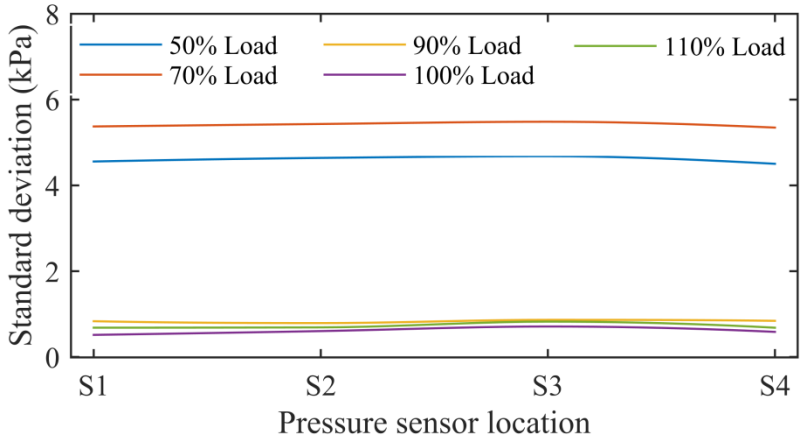

Fig. 3 Standard deviations of the fluctuating pressure values acquired from locations S1, S2, S3 and S4 at the 50%, 70%, 90%, 100% and 110% load operating conditions.

Unsteady pressure pulsations at a location S1 during the BEP (100% load) operating condition are shown in Fig. **4**. The pressure pulsations are padded around zero by subtracting the mean pressure ($\bar{p}$) from the acquired pressure (p) and are shown for 100 revolutions of the runner. Confidence intervals ± σ, ± 2σ and ± 3σ correspond to the amplitudes of ± 0.43 kPa, ± 0.86 kPa and ± 1.29 kPa, respectively. Peak-to-peak pressure amplitudes over the acquired length of pressure signal are ± 1.53 kPa, which correspond to the ± 3.5σ limit. To check randomness and repeatability, the pressure measurements were repeatedly performed at the BEP, and the calculated peak-to-peak amplitudes were below ± 3.5σ. Similarly, the pressure pulsations and confidence interval at location S1 during the 70% load operating condition are shown in Fig. **5**. The confidence intervals ± σ, ± 2σ and ± 3σ correspond to the amplitudes of ± 4.48 kPa, ± 8.96 kPa and ± 13.43 kPa, respectively. The peak-to-peak amplitudes over the recorded length correspond to the ± 3.1σ limit.

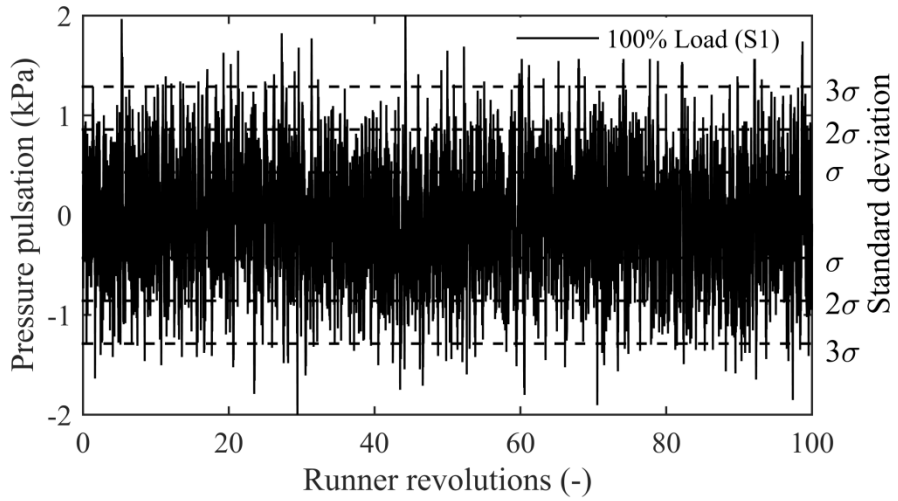

Fig. 4 Pressure pulsations at location S1 during the BEP operating condition (100% load). Dotted lines indicate 68% of the amplitudes are in the range of ± σ, 95% of the amplitudes are in the range of ± 2σ and 99.7% of the pressure amplitudes are in the range of ± 3σ.

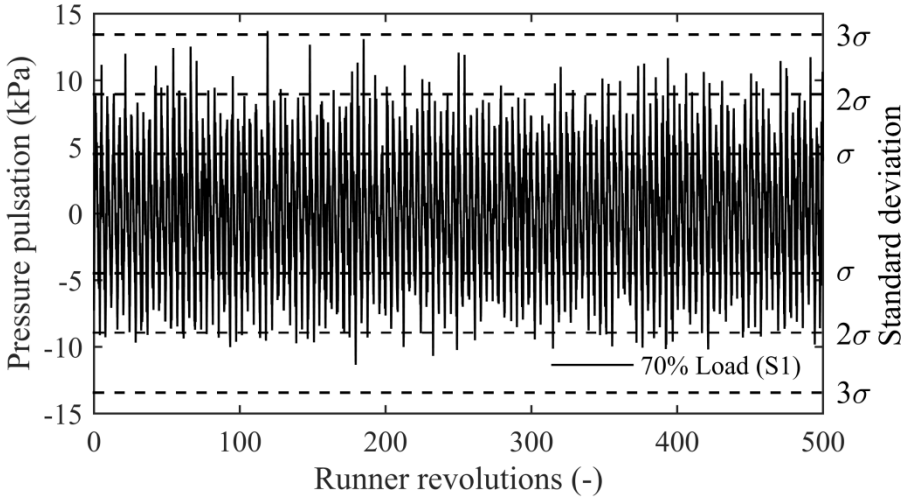

Fig. 5 Pressure pulsations at location S1 during part load operating condition (70% load). Dotted lines indicate 68% of the amplitudes are in the range of ± σ, 95% of the amplitudes are in the range of ± 2σ and 99.7% of the pressure amplitudes are in the range of ± 3σ.

Spectral analysis of all the acquired pressure values was conducted to investigate the frequency components and their amplitudes. The pressure values were sampled at 100 Hz, 500 Hz, 1 kHz, 1.5 kHz and 2.5 kHz to optimize the frequency resolution and study the amplitude dependence on the sampling rate. The estimated frequency resolution (F_s/N) was less than 0.002 Hz (< 0.05% of the runner speed). The spectral analysis showed variation of ±0.05% of $\rho \cdot E$ in the pressure amplitudes for 100 Hz and 500 Hz. For 1 kHz, 1.5 kHz and 2.5 kHz sampling rate, no variation was seen in the pressure amplitudes. Further analysis was carried out using data acquired at 2.5 kHz sampling rate to cover high frequency component such as blade passing frequency

and the harmonics. The pressure values were normalized using Equations (4) and (5) for the spectral analysis [18]:

$$p_{\mathrm{RMS}} = \sqrt{\frac{\sum_{1}^{N}(p)^2}{N}} \quad \text{(kPa)} \tag{4}$$

$$\tilde{p}_{\mathrm{E\ RMS}} = \frac{p - p_{\mathrm{RMS}}}{(\rho \cdot E)_{\mathrm{BEP}}} \quad \text{(-)} \tag{5}$$

where p is the acquired pressure in kPa, N is the number of samples used to estimate the root-mean-square (RMS), ρ is the density of water in kg m^{-3} and E is the specific hydraulic energy in J kg^{-1}; $(\rho \cdot E)_{\mathrm{BEP}}$ = 247.27 kPa. **Fig. 6** shows the amplitude spectra of the acquired time-series pressure values at a location S1. The frequencies were normalized by a frequency of the runner angular speed (5.55 Hz). Spectral analysis showed two specific frequencies, a frequency related to the vortex breakdown and another frequency related to the runner speed. At 50% and 70% load operating conditions, the observed dimensionless frequencies were 0.22 and 0.24 with their harmonics, respectively. These frequencies might be associated with the vortex rope because these frequencies are within the range of 0.2 to 0.3 times the runner speed [5, 18]. The maximum amplitude of the vortex rope frequency can be observed at 70% load operating condition. The amplitude was 6.5 times larger than the amplitude observed at 50% load. At the other operating conditions, the runner frequency (f/n = 1) with first, second and third harmonics was observed. No other frequency was observed at these conditions. The operating point with ± 10% of BEP could be relatively stable [20].

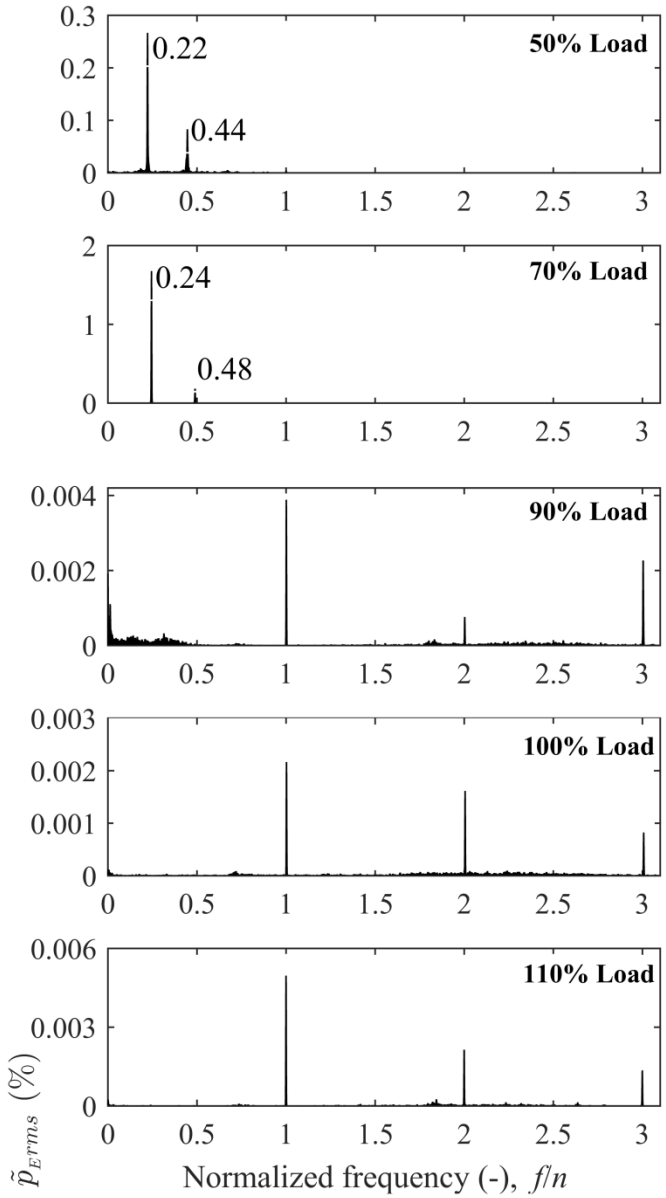

Fig. 6 Spectral analysis of the time-series pressure values at location S1 during the 50%, 70%, 90%, 100% (BEP) and 110% load operating conditions. Frequency spectra: frequencies are normalized by the runner angular speed (5.55 Hz), and the frequency span is the three times the runner rotational frequency. Full-scale amplitudes are 0.3%, 2%, 0.004%, 0.003% and 0.006% of $\rho \cdot E$ at the 50%, 70%, 90%, 100% and 110% load operating conditions, respectively; $\rho \cdot E$ = 247.27 kPa.

The time-series pressure signal usually contains frequencies related to the developed flow phenomena and random noise. It is difficult to distinguish the pressure pulsations related to flow phenomena when the amplitudes are quite similar to random noise. Techniques available in MATLAB software were applied to estimate the noise component [21]. The following statistical parameters were computed for the acquired data from the pressure sensors: signal-to-noise-ratio (SNR), total harmonic distortion (THD), and signal-to-noise and distortion ratio (SINAD) [22]. **Fig. 7** shows the SNR in the time-series pressure values at the locations S1, S2, S3 and S4. Equation (6) was used to calculate the SNR:

$$\mathrm{SNR}_{\mathrm{dB}} = 10\log_{10}\left(\frac{P_{\mathrm{signal}}}{P_{\mathrm{noise}}}\right) \quad \text{(dB)} \tag{6}$$

where P_{signal} and P_{noise} are the powers of the input signal (frequencies related to the vortex breakdown and the runner angular speed) and random noise, respectively. The estimated SNR at location S1 was -11.06 dB, 6.62 dB, -12.86 dB, -11.6 dB and -11.2 dB for the operating conditions 50%, 70%, 90%, 100% and 110% load, respectively. A positive value of SNR at 70% load operating condition indicates that the power in the amplitudes of the vortex rope frequency was greater than noise. This result suggests strong effects of the vortex rope at 70% load operating condition. Other operating conditions exhibited more noise than the actual power of the frequencies related to the vortex breakdown and the runner angular speed. **Table 2** shows the relative noise power (power of random pressure fluctuations) in the pressure signals for different operating load. The estimated noise power (dB) is normalized by the corresponding noise power (dB) at 100% load. It can be seen that the noise power at 50% and 90% load dominant in the draft tube. At 50% load, the random noise was observed between 0.6 and 80 Hz; whereas, at 90% load, the random noise was observed between 0.4 and 32 Hz. Low noise power at 70% load is due to high signal power associated with the vortex rope frequency. At 90%, 100% and 110% load, dominant signal power was attributed with the blade passing frequency of 72 Hz and up to three harmonics.

Table 2 Relative noise power in pressure signals, S1, S2, S3 and S4, for different operating load of the turbine. The noise power is normalized by the noise power at 100% load operating condition.

Location	50% load	70% load	90% load	100% load	110% load
S1	2.64	1.07	1.57	1	1.21
S2	2.61	1.02	1.59	1	1.28
S3	2.66	1.18	1.63	1	1.27
S4	2.59	1.12	1.58	1	1.29

Fig. 8 shows the THD of the acquired pressure values from the locations S1, S2, S3 and S4. THD is a measurement of the harmonic distortion of a fundamental frequency and is defined as the ratio of the sum of the powers of all harmonic components to the power of the fundamental frequency [21]. THD is most commonly defined as the ratio of the RMS amplitude of a set of higher harmonic frequencies to the RMS amplitude of the fundamental frequency, see Equation (7):

$$\mathrm{THD}_{\mathrm{dB}} = 10\log_{10}\left(\frac{\sqrt{\left(\tilde{p}_{\mathrm{E\ RMS\ f1}}\right)^2 + \left(\tilde{p}_{\mathrm{E\ RMS\ f2}}\right)^2}}{\tilde{p}_{\mathrm{E\ RMS\ f}}}\right) \quad \text{(dB)} \tag{7}$$

where $\tilde{p}_{\mathrm{E\ RMS\ f}}$, $\tilde{p}_{\mathrm{E\ RMS\ f1}}$, and $\tilde{p}_{\mathrm{E\ RMS\ f2}}$, are the amplitudes of the fundamental frequency, the first harmonic, and the second harmonic, respectively. The estimated THD at 50% and 70% load was -16 dB and -11 dB, respectively. At 50% and 70% load, the observed fundamental frequency and the first harmonic corresponded to the vortex breakdown frequency (see **Fig. 6**). The power of the first harmonic was 1/3 and 1/9 times the fundamental frequency at 50% and 70% load, respectively. The THD at the BEP and other operating conditions indicate that the harmonics have quite similar amplitudes to that of the fundamental frequency. **Fig. 9** shows the SINAD of the acquired pressure values. SINAD is a measure of the quality of a signal and is expressed as

$$\mathrm{SINAD}_{\mathrm{dB}} = 10\log_{10}\left(\frac{P_{\mathrm{signal}} + P_{\mathrm{noise}} + P_{\mathrm{distortion}}}{P_{\mathrm{noise}} + P_{\mathrm{distortion}}}\right) \quad \text{(dB)} \tag{8}$$

where P_{signal}, P_{noise} and $P_{\mathrm{distortion}}$ are the power of an input signal, noise and distortion, respectively. The pressure signals at 70% load operating conditions showed a maximum value of SINAD, indicating good quality and less distortion of the vortex breakdown frequencies. Distortion of a fundamental frequency and its harmonics can be explained by estimating the difference between the SNR and SINAD values. The minimum distortion (< 1%) is estimated at 70% load operating condition. A negative value of power (dB) at 50%, 90%, 100% and 110% load operating conditions indicates more random noise than the pure sinusoidal signal of the frequencies related to the vortex rope and the runner angular speed. Further analysis was performed at the 70% load operating condition to investigate the synchronous and asynchronous components of the vortex breakdown frequency. Moreover, a high amplitude of the vortex rope frequency was observed at the 70% load operating condition.

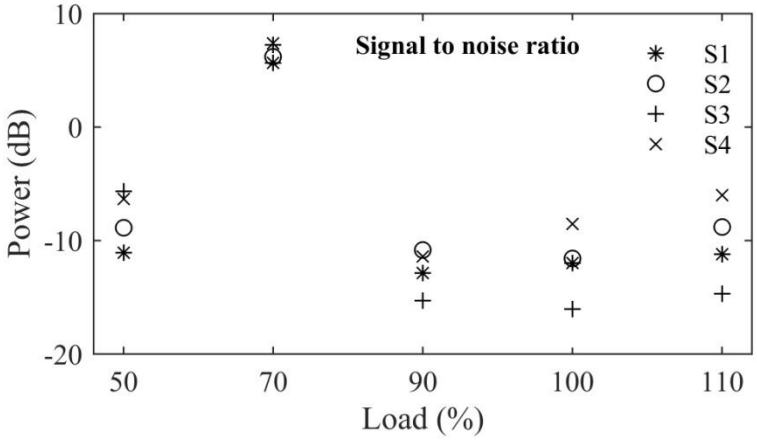

Fig. 7 Signal-to-noise ratios of the pressure values acquired at the 50%, 70%, 90%, 100% and 110% load operating conditions. S1, S2, S3 and S4 are the sensor locations in the draft tube cone at a distance 0.27·*D* from the runner outlet.

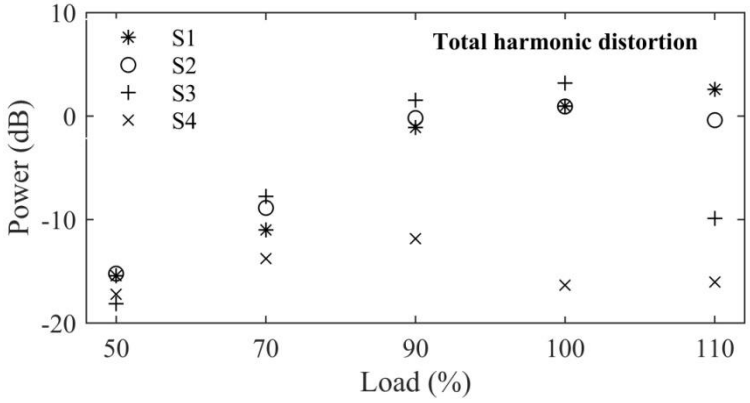

Fig. 8 Total harmonic distortion of the frequency components available in the pressure values acquired at the 50%, 70%, 90%, 100% and 110% load operating conditions. S1, S2, S3 and S4 are the sensor locations in the draft tube cone at a distance 0.27·*D* from the runner outlet.

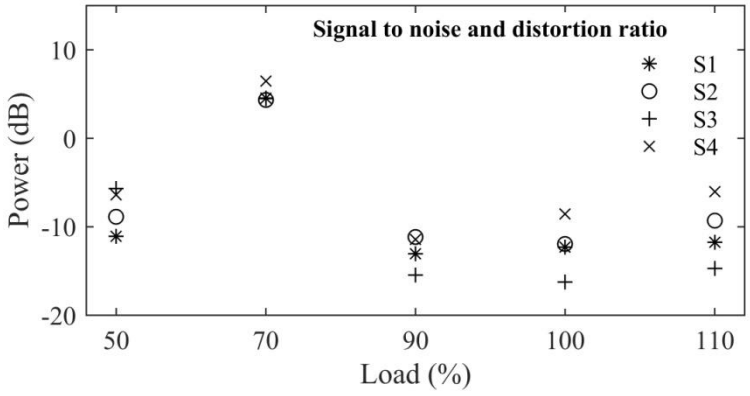

Fig. 9 Signal-to-noise and distortion of the frequency components available in the pressure values acquired at the 50%, 70%, 90%, 100% and 110% load operating conditions. S1, S2, S3 and S4 are the sensor locations in the draft tube cone at a distance 0.27·*D* from the runner outlet.

Sensors S1 and S3 were located at radial positions 180° from each other; similarly, sensors S2 and S4 were located at radial positions 180° from each other. By averaging the pressure values S1, S2, S3 and S4, the

asynchronous component of the pressure pulsations cancel out, leaving the synchronous component with random pulsation [8]. The data averaging was performed using Equation (9),

$$\bar{p}_S = \frac{\left(p_{S1} + p_{S2} + p_{S3} + p_{S4}\right)}{4} \quad \text{(kPa)} \tag{9}$$

where p_{S1}, p_{S2}, p_{S3} and p_{S4}, are the pressure values acquired from the locations S1, S2, S3 and S4, respectively. The pressure variation at the each location and the averaged pressure ($\bar{p}_S$) are shown in **Fig. 10**. The pressure variation corresponded to a frequency of vortex breakdown (f = 1.35 Hz). The pressure oscillations exhibited 90° phase difference from each other. Further, the spectral analysis of the pressure values was performed to investigate the frequency components and the related amplitudes. **Fig. 11** shows the amplitude spectrum of the pressure signals S1, S2, S3, and S4 as well as of $\bar{p}_S$ and the spectral average during the 70% load operating condition. High-amplitude frequencies correspond to the vortex breakdown frequency of 1.35 Hz. An important property of the spectrum can be seen, where the averaged pressure signal ($\bar{p}_S$) shows low amplitudes as compared to the spectral average. This observation indicates that both the asynchronous type and the random pulsation are canceled out during the averaging. This effect helps to estimate which fraction of the spectrum pertains to the random pulsations.

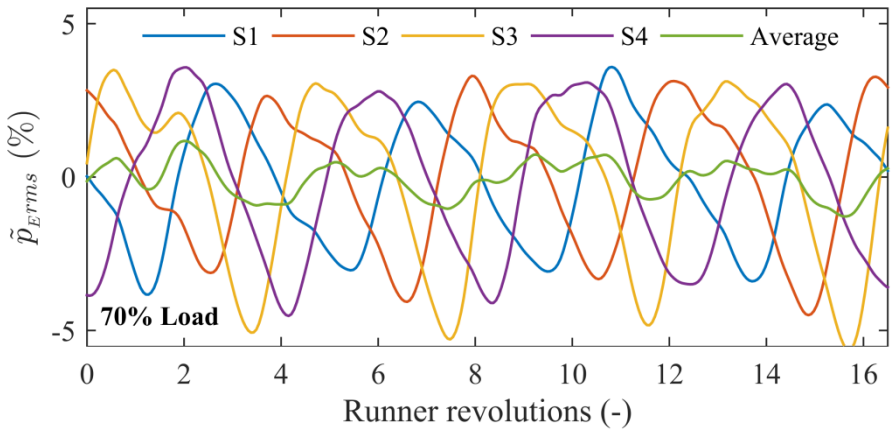

Fig. 10 Pressure variation (at the sensor locations perpendicular to the axis of draft tube cone) during the 70% load operating condition and the average pressure variation.

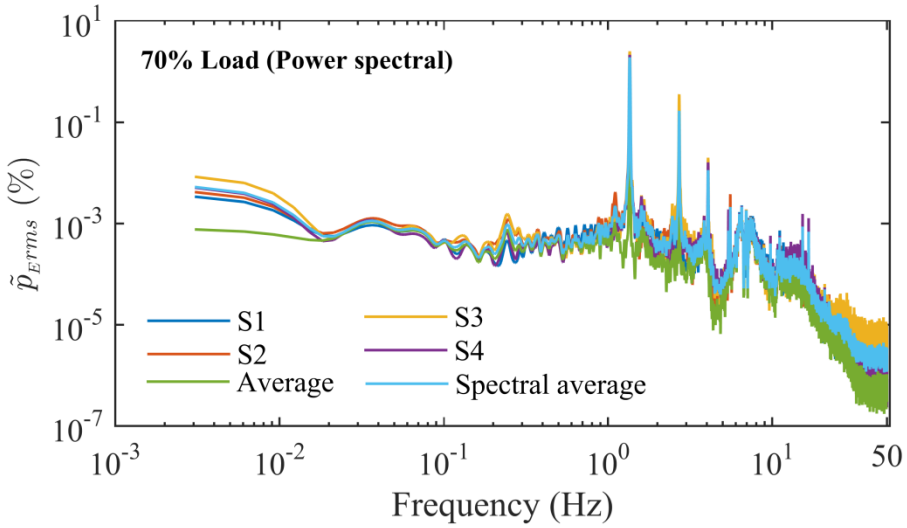

Fig. 11 Power spectral analysis of the pressure values acquired during the 70% load operating condition. Average value corresponds to the average of all four sensors at this operating condition. Spectral average is the average of the power spectra. The axes values are shown in logarithmic scale.

Both phase and coherence among the pressure signals can be estimated using multi-channel analysis. The coherence may be considered as a measure of the signal-to-noise ratio and thus be used to distinguish from the random components. **Fig. 12** shows coherence between the pressure values acquired during the 70% load operating conditions. The pressure sensors were located on the same plane at radial positions 90° from each other. Pressure sensors S1 and S3 were 180° circumferentially apart from each other; similarly, pressure sensors S2 and S4 were 180° circumferentially apart from each other. Fig. **12** (a) shows the coherence of the pressure signals S1 to S3, S2 to S4 and an average. The maximum coherence can be observed for the frequency of the vortex breakdown, 1.35 Hz, and its harmonic was related to the asynchronous component of the pressure pulsation. High coherence in the average value is associated with the high coherence in both S1-S3 and S2-S4, particularly low frequency, which can be seen in **Fig. 13**. The other property of the coherence is shown in **Fig. 12** (b), where the acquired pressure values were subtracted from the average pressure, see Equation (10) , before estimating the coherence.

$$p_{i,\,\mathrm{S}} = p_i - \bar{p}_S \quad \text{(kPa)};\ i = 1,\ 2,\ 3 \text{ and } 4 \tag{10}$$

Using this equation, random noise and synchronous components of pressure pulsation were subtracted before estimating the coherence. Completely different behavior can be observed compared to **Fig. 12** (a). This difference could be related to a pure signal being related to the rotating component of the pressure pulsations. The data shows up to four harmonics of the vortex rope frequency 1.35 Hz.

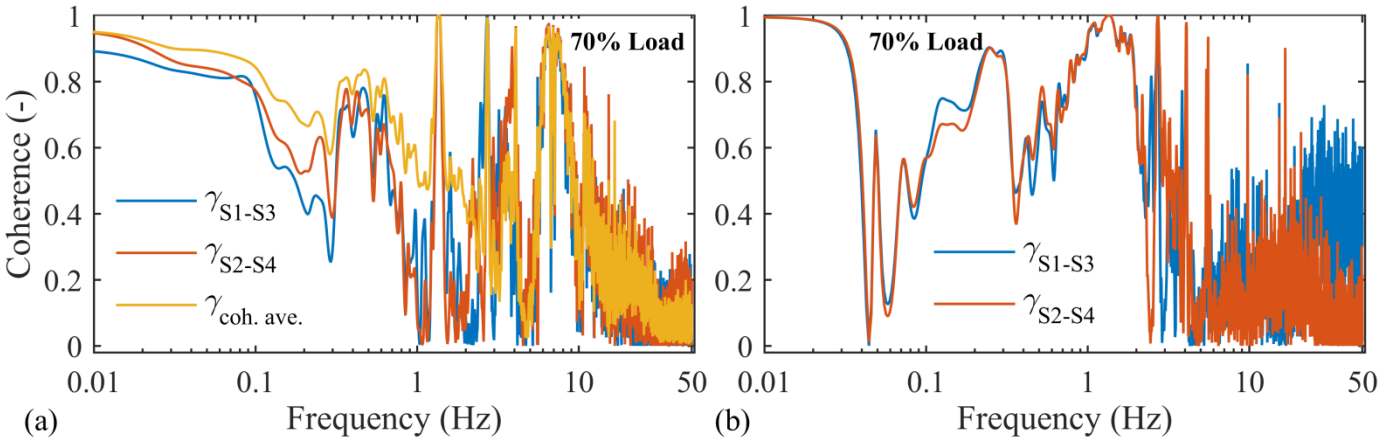

Fig. 12 Coherence of the time-series pressure values acquired during the 70% load operating condition. Locations S1, S2, S3 and S4 are perpendicular to each other on a radial plane at a distance of 0.27·D from the runner outlet. In figure (a): $p = p_i\text{-}\bar{p}_i$. In figure (b): $p = p_i\text{-}\bar{p}_S$, where, $\bar{p}_S = (p_{S1} + p_{S2} + p_{S3} + p_{S4})/4$, p_i is the acquired pressure value at the sensor locations, and i = 1, 2, 3 and 4.

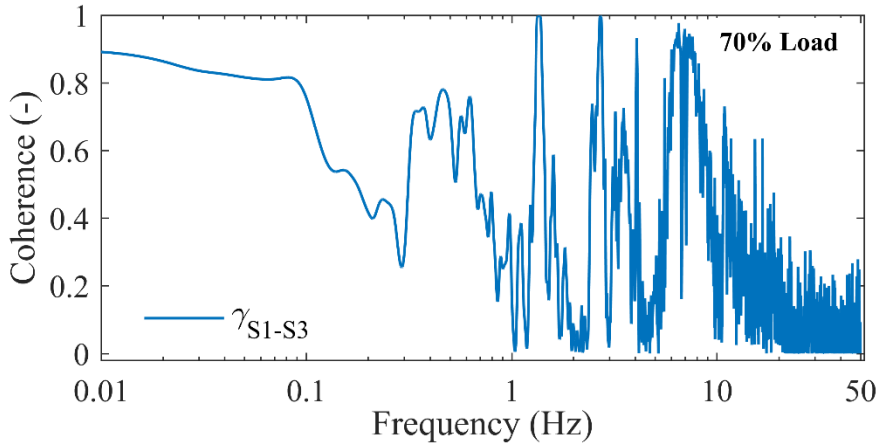

Fig. 13 Coherence of the time-series pressure values acquired during the 70% load operating condition. Locations S1 and S3 are at 180° circumferentially apart from each other at a distance of 0.27·D from the runner outlet.

To estimate the amplitudes of synchronous and asynchronous type pressure pulsations, power spectral analysis was conducted. **Fig. 14** shows amplitude spectra of synchronous and asynchronous components at the 70% load operating condition. The amplitude spectra of pressure signals S1 and S2 are shown in **Fig. 14** (a) and **Fig. 14** (b), respectively. The synchronous and asynchronous components were computed using Equations (11) and (12), respectively [7, 8].

$$p_{syn} = \frac{S1 + S3}{2} \quad \text{(kPa)} \tag{11}$$

$$p_{asyn} = \frac{S1 - S3}{2} \quad \text{(kPa)} \tag{12}$$

A vortex rope frequency (f/n = 0.24) and its harmonic can be observed at both locations. The amplitudes at both locations are almost identical. By taking the average of the pressure values from opposite locations, the rotating periodic type pressure pulsations cancel each other out, whereas the axial (including non-periodic) and random pressure pulsations remain, as shown in **Fig. 14** (c). The amplitude of the fundamental frequency was reduced from 2% to 0.1% of $\rho \cdot E$, whereas the amplitude of the first harmonic was almost identical to that observed before averaging. As shown in **Fig. 14** (d), the amplitudes of the fundamental frequency were similar, whereas the amplitude of the first harmonic almost disappeared. Asynchronous type pressure pulsations have a full-scale amplitude approximately 2% of $\rho \cdot E$. The amplitude of the asynchronous component is approximately 20 times larger than those of the synchronous component in this turbine at the 70% load operating condition. A similar variation was observed for the other sensor locations S2 and S4; this variation is not discussed in this paper.

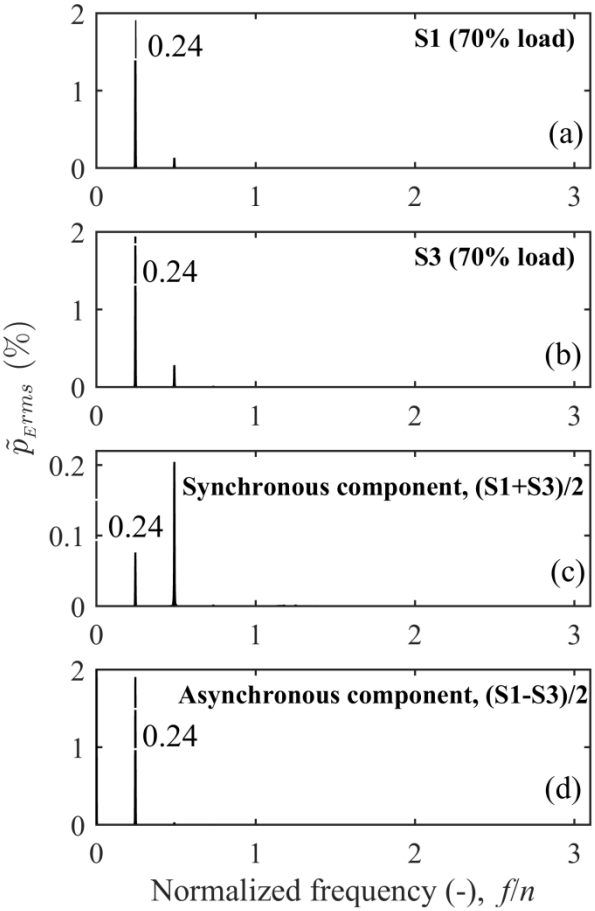

Fig. 14 Spectral analysis of pressure signals S1 and S3 located at radial positions 180 degrees from each other. The synchronous component of the pressure pulsations is computed as (S1+S3)/2, and the asynchronous component is computed as (S1-S3)/2. The maximum amplitude spectrum is 2% of $\rho \cdot E$. The peak at f/n = 0.24 corresponds to a frequency of vortex breakdown at the measurement location.

3.2 Pressure pulsations: Francis turbine-2

Unsteady pressure measurements were performed on another Francis turbine located at Øvre Leirfossen. The turbine runner was mounted along the horizontal axis and directly coupled with the generator. The runner was operating at the synchronous speed, 6.25 Hz, during the measurements. Four pressure sensors were mounted on the wall of the draft tube cone at equal radial positions from each other. Two sensors, S1 and S4, were located below a horizontal plane passing through the center of the runner. The other two sensors, S2 and S3, were located above the horizontal plane (see **Fig. 1**). The sensors are numbered in the direction of the runner angular rotation. The measurements were conducted at five operating points: 50%, 70%, 90%, 100% and 110% load of BEP. BEP corresponds to the 100% load operating condition. **Fig. 15** shows the average pressure at the locations S1, S2, S3 and S4 of the five operating points. The pressure sensors mounted below the axis of the runner exhibited higher pressure than the other two sensors mounted above the axis for all operating points. The minimum pressure (32 kPa absolute) was found at location S3 during the 110% load (high load) operating condition. The maximum pressure was found at location S1 for the 70% load operating condition. Variable pressure along the radial position indicates the asymmetrical flow condition at the runner outlet. The standard deviations of the acquired pressure values at the 50%, 70%, 90%, 100% and 110% load operating points are shown in **Fig. 16**. The maximum standard deviation (6.67 kPa) was observed for the 50% load operating point, and the minimum (< 1 kPa) standard deviation was observed for the BEP. At 70% load, the standard deviation was 5 kPa and 4 kPa at locations S1 and S4, respectively. Higher standard deviations at locations S1 and S2 indicate larger pressure pulsations compared with those at locations S3 and S4.

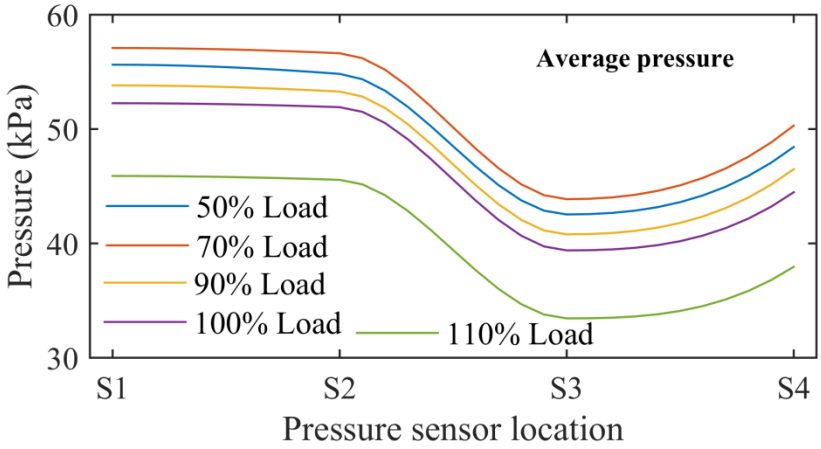

Fig. 15 Average pressure loading at locations S1, S2, S3 and S4 during the 50%, 70%, 90%, 100% and 110% load operating conditions. The sensors are numbered in the direction of the runner rotation. S1 and S2 are located below a horizontal plane passing through the runner axis; S3 and S4 are located above the horizontal plane passing through the runner axis. The locations of the pressure sensors are shown in **Fig. 1**.

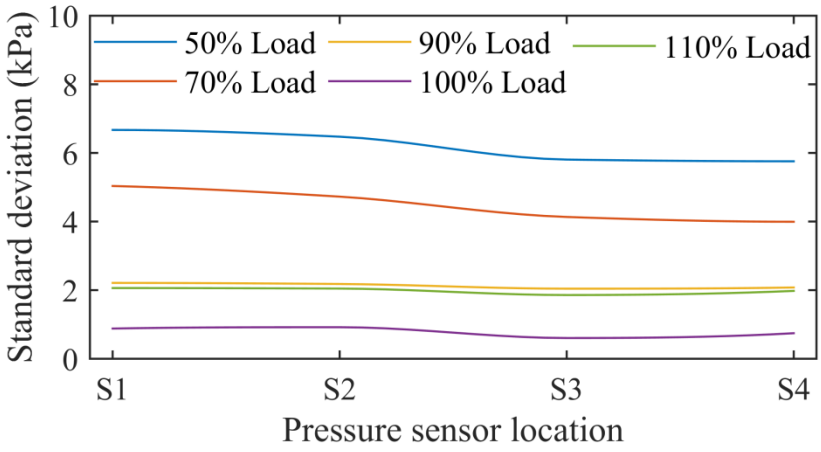

Fig. 16 Standard deviations of the unsteady pressure pulsations acquired at the locations S1, S2, S3 and S4 during the 50%, 70%, 90%, 100% and 110% load operating conditions.

Spectral analysis of the acquired pressure values was performed to investigate the low frequency amplitude spectra. **Fig. 17** shows the frequency analysis results at location S1 during the 50%, 70%, 90%, 100% and 110% load operating conditions. The frequencies were normalized by the runner speed (6.25 Hz), and the amplitudes were normalized by reference pressure observed at the BEP, $\rho \cdot E$ = 319.9 kPa. The scale for the amplitude spectra is different for each operating condition: 0.3% of $\rho \cdot E$ for the 50%, 70% and 110% load operating conditions and 0.03% of $\rho \cdot E$ for the 90% and 100% load operating conditions. The maximum amplitude was found for the frequency of 0.27 at the 70% load operating condition, which may correspond to a frequency of the vortex rope in the draft tube. At the 50% load operating condition, a high-amplitude frequency of 0.16 was observed, which might be the fundamental frequency of the vortex rope. A harmonic at a frequency of 0.32 was observed with very low amplitude (< 0.001% of $\rho \cdot E$). At the upper part load (90%

load), the observed frequency related to vortex rope was 0.25. At the BEP, no frequency with high amplitude was observed. At the 110% load operating condition, a frequency of 0.28 was observed, which may be related to the vortex rope. The amplitude was 30 times lower than the amplitude observed for the 70% load operating condition.

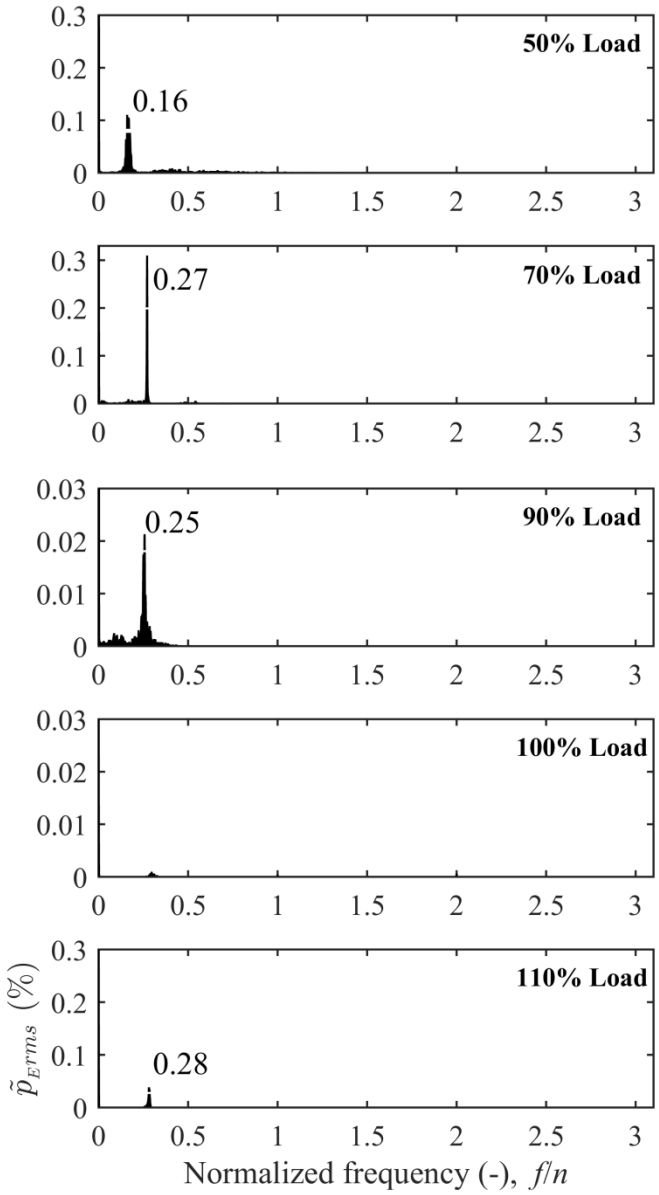

Fig. 17 Spectral analysis of time-series pressure values at a location S1 during the 50%, 70%, 90%, 100% (BEP) and 110% load operating conditions. Frequency spectra: frequencies are normalized by the runner angular speed (6.25 Hz), and the frequency span is the three times the runner rotational frequency. The full-scale amplitudes are 0.3% of $\rho \cdot E$ at the 50%, 70% and 110% load operating conditions and are 0.03% of $\rho \cdot E$ at the 90% and 100% load operating conditions, $\rho \cdot E$ = 319.9 kPa.

To investigate the random noise and purity of the pressure signals, SNR analysis was conducted on all the pressure values. **Fig. 18** shows the SNR of pressure signals S1, S2, S3 and S4 for the 50%, 70%, 90%, 100% and 110% load operating conditions. Except for the 70% load operating condition, the power was below zero

dB at all operating conditions. This result indicates that the power related to a frequency of the vortex breakdown is greater than the random noise at the 70% load operating condition. The maximum noise can be observed at the 50% and 100% load operating conditions, with values of -11 dB and -16 dB, respectively. Because the maximum amplitude was estimated at the 70% load operating condition, further analysis was conducted for this operating point. Noise power for the S1, S2, S3 and S4 pressure signals is shown in **Table 3**. The noise power is normalized by the noise power at 100% (BEP) load. In this turbine, random noise at 50% and 90% load is dominant similar to the turbine-1; however, the noise is approximately 20-40% higher than the turbine-1 case. Furthermore, the high amplitude noise band is small in this turbine. At 50% load, the high amplitude noise is observed between 0.7 Hz and 32 Hz; at 90% load, the high amplitude noise is observed between 0.1 Hz and 19 Hz.

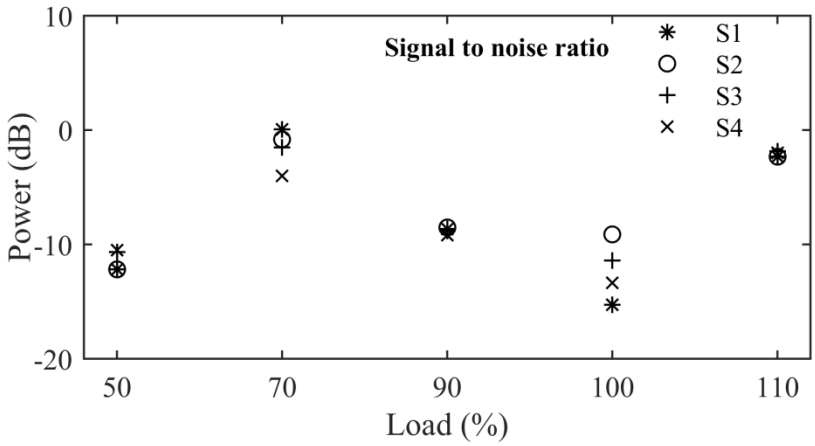

Fig. 18 Signal-to-noise ratio of the pressure values acquired at the 50%, 70%, 90%, 100% and 110% load operating conditions. S1, S2, S3 and S4 are the sensor locations in the draft tube cone in the direction of the runner rotation.

Table 3 Relative noise power in pressure signals, S1, S2, S3 and S4, for different operating load of the turbine. The noise power is normalized by the noise power at 100% load operating condition.

Location	50% load	70% load	90% load	100% load	110% load
S1	4.16	1.39	2.71	1	1.91
S2	4.12	1.46	2.69	1	1.86
S3	4.15	1.41	2.74	1	1.88
S4	4.09	1.48	2.68	1	1.94

The average pressure variations at locations S1, S2, S3 and S4 at the 70% load operating conditions are shown in **Fig. 19**. The pressure variation is shown for 16 revolutions of the runner, which is approximately 4 sinusoidal periods of the vortex rope. The pressure values were averaged using samples of one complete

revolution of the runner. The pressure variation corresponded to a vortex rope frequency of 1.68 Hz. The phase difference between the pressure signals was 90°. A total of four pressure sensors were mounted at 90° radial positions from each other in the radial direction starting from S1 and going to S4. The pressure signals included both the synchronous and asynchronous components of the pressure pulsations. The average pressure signal exhibited a variation similar to that observed for Francis turbine-1. The average pressure signal includes the random component of pressure pulsations, and the other components may be related to the synchronous type pressure pulsations. Spectral analysis of the pressure values acquired from locations S1 and S3 is shown in Fig. **20**. The pressure sensors S1 and S3 were located at radial positions 180° from each other on the same plane. Location S1 was below the horizontal plane passing through the axis of the runner, and location S3 was above the horizontal plane. Therefore, a low amplitude at location S3 was expected, which can be observed by comparing the amplitude of the vortex breakdown frequency of 0.27 in Fig. **20** (a) and (b). Equations (11) and (12) were used to estimate the synchronous and asynchronous components of the pressure pulsations, respectively. The amplitude of the synchronous component was almost identical to the amplitude observed at locations S1 and S3. The amplitude of the asynchronous component was reduced by 50%, indicating that the synchronous component had a large effect on the draft tube flow.

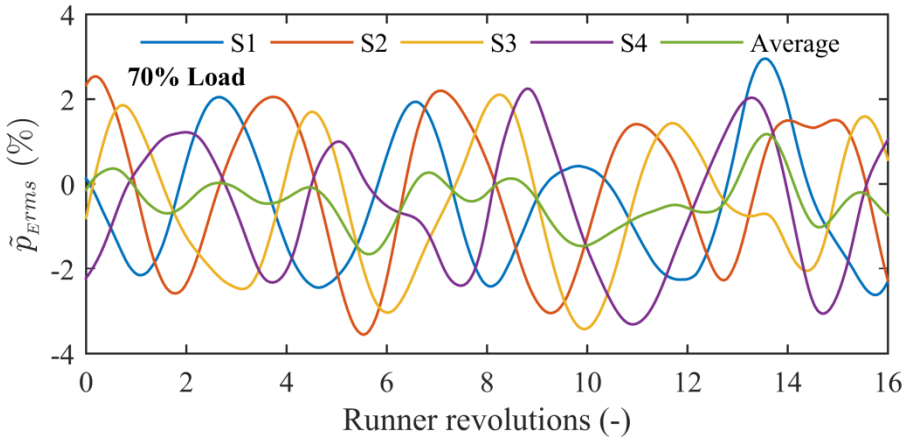

Fig. 19 Average pressure variations at locations S1, S2, S3 and S4 with respect to the runner angular movement at the 70% load operating condition. The oscillations correspond to the frequency of the vortex breakdown (1.68 Hz) in the draft tube.

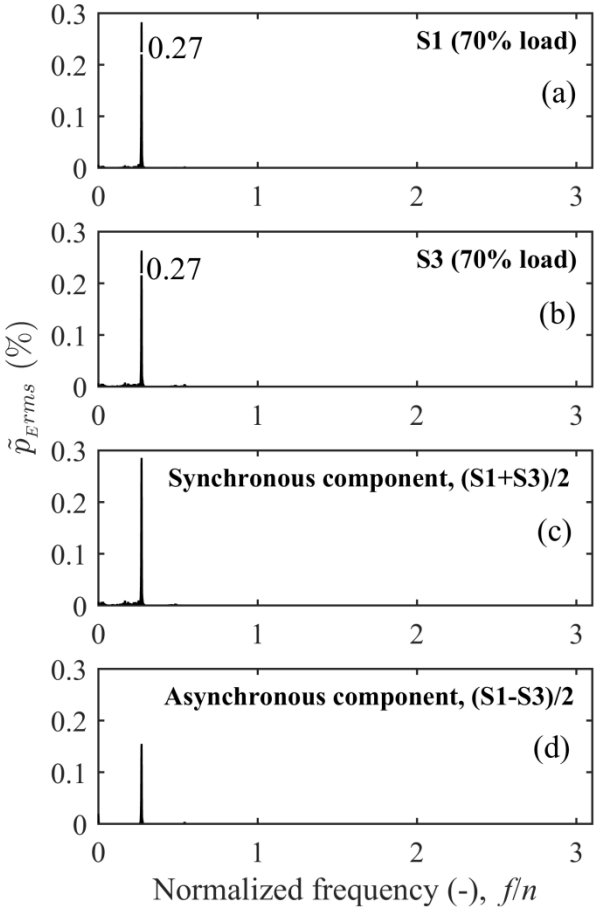

Fig. 20 Spectral analysis of pressure signals S1 and S3 located at radial positions 180 degree from each other. The synchronous component of the pressure pulsations is computed as (S1+S2)/2, and the asynchronous component is computed as (S1-S2)/2. The maximum amplitude spectrum is 0.3% of $\rho \cdot E$. The peak at f/n = 0.27 correspond to the frequency of the vortex breakdown at the measurement location.

4. Conclusion

Unsteady pressure measurements were performed on two prototype Francis turbines. Turbine-1 and turbine-2 were vertical and horizontal axis-type turbines, respectively. Four pressure sensors were mounted onto the surface of the draft tube cone at a distance $0.27 \cdot D$ downstream of the runner. Pressure values were acquired at five operating points: 50%, 70%, 90%, 100% and 110% of BEP load, where 100% corresponds to BEP load. Repeated measurements were conducted to check the repeatability of the data, and the data were sampled at 100 Hz, 500 Hz, 1 kHz, 1.5 kHz and 2.5 kHz to check the influence of the sampling rate on the amplitudes. The investigations included statistical analysis, spectral analysis, coherence and cross correlation between the signals.

Statistical analysis demonstrated that the peak-to-peak amplitudes of the pressure pulsations are within the limit of 0.6% of the head at the BEP and 5.5% of the head at the 70% load. Further analysis showed that the

amplitude of a frequency related to the draft tube vortex rope is within the limit of 3.5% to 5.3% of the head. Spectral analysis of all the acquired pressure values was performed, with the observed frequencies of the vortex rope ranging from 0.22 to 0.3 times the runner speed at all operating points, except at the BEP. Coherence analysis showed that the phase between the opposite pressure signal was approximately 178° for the frequency corresponding to asynchronous-type pressure pulsations. Spectral analysis showed a higher amplitude of the synchronous component in the horizontal axis turbine (turbine-2) compared with the amplitude observed in the vertical axis turbine (turbine-1). The maximum amplitudes were observed at the 70% load for both turbines. The full-scale amplitudes were 1.8% and 0.3% of $\rho \cdot E$ for the vertical axis and horizontal axis turbines, respectively. In the vertical axis turbine, amplitudes of asynchronous pressure pulsations were 20 times larger than those of the synchronous component; whereas, in the horizontal axis turbine, the amplitudes of asynchronous pressure pulsations were two times smaller than those of the synchronous component. This indicates that the asynchronous pressure pulsations have strong influence on the flow field in the vertical draft tube and the opposite is true for the horizontal one. Furthermore, unlike horizontal axis turbine, vertical axis turbine showed harmonics of both types of pressure pulsations. The reduced effect of the asynchronous pressure pulsations in the horizontal axis turbine may be attributed to the orientation of the draft tube in addition to the swirling flow leaving from the runner. The orientation of draft tube outlet from the elbow may be playing certain role and the reflection of the pressure/standing waves between draft tube elbow and the outlet.

Acknowledgements

The presented work was performed under the research project “Efficiency Measurement at Leirfossen Kraftverk”. The project was financially supported by Statkraft AS, Norway. Low head Francis turbines located at Nedre Leirfossen and Øvre Leirfossen were investigated. Hydraulic efficiency measurements and unsteady pressure measurements were performed.

Nomenclature

BEP = Best efficiency point

D = runner outlet diameter (m)

E = Specific hydraulic energy (J kg^{-1})

F_s = Data sampling rate (Hz)

f = Frequency (Hz)

H = Head (m)

IEC = International Electrotechnical Commission

N = Number of samples

N_{QE} = Specific speed (-)

n = Runner angular speed (rps)

n_{ED} = Speed factor (-)

P = Power (MW), signal power (dB)

p = Pressure (kPa)

$\bar{p}$ = Average pressure (kPa)

$\bar{p}_S$ = Average pressure (kPa), $\bar{p}_S$ = (S1+S2+S3+S4)/4

$\tilde{p}_{eff}$ = Standard deviation (kPa)

Q = Discharge (m^3 s^{-1})

Q_{ED} = Discharge factor (-)

RMS = Root-mean-square

rps = Revolutions per second

SINAD = Signal-to-noise and distortion ratio

SNR = Signal-to-noise-ratio

S1, S2, S3 and S4 = Locations of the pressure sensors mounted in a draft tube cone

THD = Total harmonic distortion

Greek letters

σ = Standard deviation (kPa)

ρ = Water density (kg m^{-3})

Subscripts

asyn = Asynchronous component (rotating) of the pressure pulsation

i = integer, where i = 1, 2, 3 and 4

syn = synchronous component (axial) of the pressure pulsation

References

[1] Sawin JL, Sverrisson F, Martinot E. Renewables 2014 global status report. In: Mastny L, editor. REN21 Secretariat, Paris, France: Renewable Energy Policy Network for 21st Century; 2014. p. 215.

[2] Trivedi C, Gandhi B, Cervantes M. Effect of transients on Francis turbine runner life: A review. J Hydraul Res. 2013;51:121-32. doi: 10.1080/00221686.2012.732971.

[3] Keck H, Weiss T, Michler W, Sick M. Recent developments in the dynamic analysis of water turbines. Proceedings of the Institution of Mechanical Engineers, Part A: Journal of Power and Energy. 2009;223:415-27. doi: 10.1243/09576509JPE578.

[4] Thapa BS, Thapa B, Dahlhaug OG. Empirical modelling of sediment erosion in Francis turbines. Energy. 2012;41:386-91. doi: 10.1016/j.energy.2012.02.066.

[5] Dörfler P, Sick M, Coutu A. Flow-induced pulsation and vibration in hydroelectric machinery. First ed: Springer; 2013.

[6] Magnoli MV. Numerical simulation of pressure oscillations in large Francis turbines at partial and full load operating conditions and their effects on the runner structural behaviour and fatigue life [Ph. D.]: Technische Universitat Munchen; 2014.

[7] Bosioc AI, Susan-Resiga R, Muntean S, Tanasa C. Unsteady pressure analysis of a swirling flow with vortex rope and axial water injection in a discharge cone. J Fluid Eng-T Asme. 2012;134:081104. doi: 10.1115/1.4007074.

[8] Doerfler P, Ruchonnet N. A statistical method for draft tube pressure pulsation analysis. IOP Conference Series: Earth and Environmental Science, 26th IAHR Symposium on Hydraulic Machinery and Systems, IOP Publishing, 2012: 062002.doi: 10.1088/1755-1315/15/6/062002.

[9] Ciocan GD, Iliescu MS, Vu TC, Nennemann B, Avellan F. Experimental study and numerical simulation of the flindt draft tube rotating vortex. J Fluid Eng-T Asme. 2007;129:146-58. doi: 10.1115/1.2409332.

[10] Wang ZW, Zhou LJ. Simulations and measurements of pressure oscillations caused by vortex ropes. J Fluid Eng-T Asme. 2006;128:649-55. doi: 10.1115/1.2201631.

[11] Shingai K, Okamoto N, Tamura Y, Tani K. Long-period pressure pulsation estimated in numerical simulations for excessive flow rate condition of Francis turbine. J Fluid Eng-T Asme. 2014;136:071105. doi: 10.1115/1.4026584.

[12] Foroutan H, Yavuzkurt S. Flow in the simplified draft tube of a Francis turbine operating at partial load—part ii: Control of the vortex rope. Journal of Applied Mechanics. 2014;81:061011. doi: 10.1115/1.4026818.

[13] Foroutan H, Yavuzkurt S. Flow in the simplified draft tube of a Francis turbine operating at partial load-part I: Simulation of the vortex rope. J Appl Mech-T Asme. 2014;81:8. doi: 10.1115/1.4026817.

[14] Escaler X, Ekanger JV, Francke HH, Kjeldsen M, Nielsen TK. Detection of draft tube surge and erosive blade cavitation in a full-scale Francis turbine. J Fluid Eng-T Asme. 2015;137:011103. doi: 10.1115/1.4027541.

[15] Tridon S, Barre S, Ciocan G, Segoufin C, Leroy P. Discharge imbalance mitigation in Francis turbine draft-tube bays. J Fluid Eng-T Asme. 2012;134:8. doi: 10.1115/1.4006064.

[16] Tridon S, Barre S, Ciocan GD, Tomas L. Experimental analysis of the swirling flow in a Francis turbine draft tube: Focus on radial velocity component determination. Eur J Mech B-Fluid. 2010;29:321-35. doi: 10.1016/j.euromechflu.2010.02.004.

[17] Kurokawa J, Imamura H, Choi Y-D. Effect of j-groove on the suppression of swirl flow in a conical diffuser. J Fluid Eng-T Asme. 2010;132:071101. doi: 10.1115/1.4001899.

[18] IEC 60193. Hydraulic turbines, storage pumps and pump-turbines: Model acceptance tests. International standard. Second ed. 3, rue de Varembé, PO Box 131, CH-1211 Geneva 20, Switzerland: International Electrotechnical Commission; 1999. p. 578.

[19] IEC 41. Field acceptance tests to determine the hudraulic performance of hydraulic turbines, storage pumps and pump-turbines. International standard. Third ed. 3, rue de Varembé, PO Box 131, CH-1211 Geneva 20, Switzerland: International Electrotechnical Commission; 1991. p. 430.

[20] Brekke H. Performance and safety of hydraulic turbines. IOP Conference Series: Earth and Environmental Science, 25th IAHR Symposium on Hydraulic Machinery and Systems, IOP Publishing, 2010: 012061.doi: 10.1088/1755-1315/12/1/012061.

[21] MATLAB. Signal processing toolbox reference guide. 3 Apple Hill Drive, Natick, MA 01760-2098: The MathWorks, Inc.; 2015. p. 1810.

[22] Proakis JG, Manolakis DG. Digital signal processing: Principles, algorithms, and applications. Englewood Cliffs1996.